EEET ECOLOGICAL ENGINEERING & ENVIRONMENTAL TECHNOLOGY

Ecological Engineering & Environmental Technology 2024, 25(1), 22–45
https://doi.org/10.12912/27197050/173567
ISSN 2719-7050, License CC-BY 4.0

Received: 2023.10.04
Accepted: 2023.11.18
Published: 2023.12.14

Groundwater Quality Assessment in the Coastal Mediterranean Aquifer of Northeastern Morocco – A GIS-Based Approach

Sara Bouhout[1,2], Khadija Haboubi[2], Yahya El Hammoudani[2*], Aouatif El Abdouni[1,2], Chaimae Haboubi[2], Fouad Dimane[2], Issam Hanafi[2], Mohamed Salahdine Elyoubi[1]

[1] Laboratory of Organic Chemistry, Catalysis and Environment, Faculty of Science, Ibn Tofail University, Kénitra, Morocco

[2] Laboratory of Engineering Sciences and Application, National School of Applied Sciences - Al Hoceima, Abdelmalek Essaadi University, Morocco

* Corresponding author's e-mail: elhammoudani5@gmail.com

ABSTRACT

Groundwater quality degradation is a pressing concern in semi-arid coastal regions, exemplified by the Ghiss-Nekor aquifer in northeastern Morocco, spanning 100 km². This study adopts a comprehensive approach, utilizing chloro-alkaline indices, hydrochemical facies diagrams, the water quality index (WQI), and the synthetic pollution index (SPI) to assess the groundwater quality and its evolution. Key findings reveal that the Ghiss-Nekor groundwater is brackish, primarily suitable for irrigation due to high total dissolved solids (TDS). Salinization stems from reverse cation exchange, as indicated by hydrochemical analyses. WQI assessments highlight the inadequacy of this groundwater for drinking purposes, with SPI classifying 54% of wells as moderately polluted. Fine particles mitigate marine intrusion in the northwest. Overlaying land-use and electrical conductivity maps identifies the areas with poor-quality groundwater, notably near an unregulated landfill, a coastal tourist site, and a wastewater treatment facility. Ionic analysis identifies multiple saline sources, with nitrate and sulfate contributions standing out. While the study offers valuable insights, limitations include the need for ongoing data collection and source identification challenges. Nonetheless, the research underscores the urgency of effective water management, particularly around the landfill site situated above permeable deposits, offering an innovative approach with global applicability for addressing groundwater quality issues in semi-arid coastal areas.

Keywords: coastal aquifers, northeastern Morocco, landfill site, WQI, synthetic pollution index, drinking purposes, marine intrusion.

INTRODUCTION

The availability of clean and reliable groundwater is vitally important to ensure food security, public health and social development, since 2.5 billion people around the world basically rely on aquifers for their drinking-water supply (Gao, 2020). Yet, in recent times, groundwater quality deterioration has become an increasingly prominent issue related to the increasing population growth rate and unplanned urbanization leading to intensive exploitation of aquifers to meet the growing water demand. These constraints, further exacerbated in coastal areas where almost 70% of the global population lives (Akoteyon, 2018) and within arid/semi-arid regions characterized by the scarcity of surface-water bodies, are associated with groundwater quality degradation, particularly by salinization. Salinization of groundwater could arise from multiple sources, either naturally occurring such as weathering of evaporite minerals and brines, presence of trapped fossil seawater and accumulation of sea-spray or in conjunction with anthropogenic sources including improper sewage disposal, application of fertilizers and pesticides as well as over-pumping (Bourjila,

2023, Radouane, 2023). Moreover, marine intrusion is another potential source of salinization in coastal aquifers; the mixing zone between freshwater and intruding seawater, as the most vulnerable and chemically active part of these aquifers, can migrate landward under the influence of unmonitored pumping activities occurring close to the shoreline (Ghalit, 2017, Hajji, 2022). Shallow alluvial aquifers are more vulnerable and prone to the abovementioned salinity hazards; their lithologies, mainly constituted by highly permeable unconsolidated sediments, enable a rapid and easy infiltration of contaminants to the water table (Rupias, 2021). The combined interaction of salinization factors could eventually induce irreversible degradation in groundwater chemistry, but also adds a high complexity level to the task of elucidating the origin of groundwater salinity (Abu-Alnaeem, 2018). In this context, the complementary use of chemical analysis tools is essential for a proper investigation and characterization of groundwater chemistry as well as the associated salinization mechanisms. A hydrogeochemical method, which involves the assessment of major ions in groundwater has been widely used in earlier studies, since it is characterized by a high-resolution capacity at an affordable cost (Benaissa, 2022, Elabdouni, 2022, Bouhout, 2023). The most commonly used hydrochemical techniques include: analysis of molar ionic ratios (Belghiti, 2013, Ngouala, 2016, Benaissa, 2020), estimation of seawater fraction and ionic deltas (El Hammoudani, 2019, El Hammoudani, 2020, Dimane, 2021, El Hammoudani, 2023) as well as several graphical techniques to visually interpret the resulting chemical characteristics, such as scatter plots of the physico-chemical parameters, piper trilinear diagram and the Hydrochemical Evolution Facies diagram. Additionally, over the last decade, authors of multiple published investigations, carried out in coastal areas under arid and semi-arid conditions, focused on the assessment of the groundwater quality, pollution status and its usability for different purposes through the combined application of water quality index (WQI), synthetic pollution index (SPI) and geographical information system (GIS) (Chukwu, 2023, Laonamsai, 2023, Saleh, 2023). The purpose of WQI, as a common mathematical tool, is to merge complex data including physical, chemical and biological water-quality parameters to generate a composite index that reflects the overall water quality in a given location, which is understandable and easy to interpret for decision makers (Kanga, 2020).

Specifically in Morocco, groundwater salinization processes are documented in numerous papers; (Neverre, 2022, Das, 2023, Saleh et al., 2023) successfully employed the ratio Br^-/Cl^-, stable isotopes and electrical resistivity tomography, respectively, in conjunction with the hydrochemical facies evolution diagram to identify groundwater mineralization sources and to explore the response of coastal aquifers within Essaouira basin (Western Morocco) and Chaouia region (north-central Morocco) to seawater intrusion. Bourjila et al., 2023 attempted to estimate the level of groundwater pollution and evaluate the adequacy of groundwater quality for drinking and irrigation purposes, within Essaouira basin (Western Morocco) and Bokoya Massif (Central Rif, Northeastern Morocco), by the combined application of Groundwater Quality Index and other quality assessment methods, including Wilcox and Richards's plots and Geographical Information System. Recently, Ouhamdouch (2021) provided a large-scale overview of groundwater salinization in thirteen Moroccan coastal aquifers; the authors examined the main salinity processes in each aquifer and concluded that the groundwater in Moroccan coastal areas shows significant signs of quality degradation; moreover, they identified the following mechanisms of groundwater salinization: (1) groundwater salinity is increasing in the southern areas due to drought periods, massive groundwater exploitation and intensive agricultural practices, (2) in northern Morocco, aquifers are more affected by climate change that led to sea-level rise and inland advancement of seawater wedge. Concerning the Mediterranean coastal aquifers in Morocco, groundwater mineralization levels increase from the northwest towards the northeast due to arid climate conditions and intense human activities prevailing in the eastern regions compared to the western areas of the Mediterranean coast, dominated by mountainous structures.

In this paper, the Ghiss-Nekor Mediterranean plain aquifer, in northeastern Morocco, was selected as a case study given its environmental and economic significance; it is the highest-yielding source of freshwater supplies used for irrigation of over 5000 ha and for domestic purposes of the Al-Hoceima city and its peripheries (Abdouni, 2021, Bouhout, 2022, Bouhout et al., 2023). Among the studies in which researchers focused

on groundwater quality within the Ghiss-Nekor plain, (Al Naeem, 2019) pointed out the combined contribution of uncontrolled exploitation, anthropogenic pollution as well as the hydrogeological, climatic and tectonic settings to the deterioration of groundwater quality, through the interpretation of chemical and isotopic findings along with the application of statistical approaches. However, so far, no thorough investigation was conducted concerning the impact of land use patterns on hydrochemistry and contamination of groundwater in the study area. Therefore, the specific aims of this study were to: (1) ascertain the current groundwater quality status and its suitability for domestic and agricultural usage, (2) synthesize the available groundwater quality data and implement the findings in a GIS environment to delineate the spatial variation of the overall groundwater quality status, (3) demarcate the mechanisms controlling groundwater geochemistry that gave rise to different water types in the study area, (4) estimate the extent of saline intrusion and assess the effects caused by land-use practices on groundwater composition.

MATERIALS AND METHODS

General features of the study area

The Ghiss-Nekor coastal plain, investigated in this study, is situated about 12 kilometers to the southeast of Al-Hoceima city, in the northeastern part of Morocco (Fig. 1). This alluvial plain, positioned between latitudes 35°13', 35°05' and 35°12' North, and longitudes 3°46',3°49' and 3°54' West (Dimane, 2017, El Hammoudani et al., 2023), occupies an area of 100 km² and is drained by the Nekor and Ghiss major rivers –along with their smaller tributaries –-; Oued Nekor runs across the center of the plain along a length of 15 kilometers, while a portion of the Ghiss river crosses the northwestern edge of the plain on a length of 3 kilometers (Elabdouni, 2020, Andaloussi, 2021, El Abdouni, 2021, Fernine, 2022) . The study area has been marked as a major agricultural plain of the Al-Hoceima Province. Another important aspect is related to tectonic activity; the Ghiss-Nekor plain is

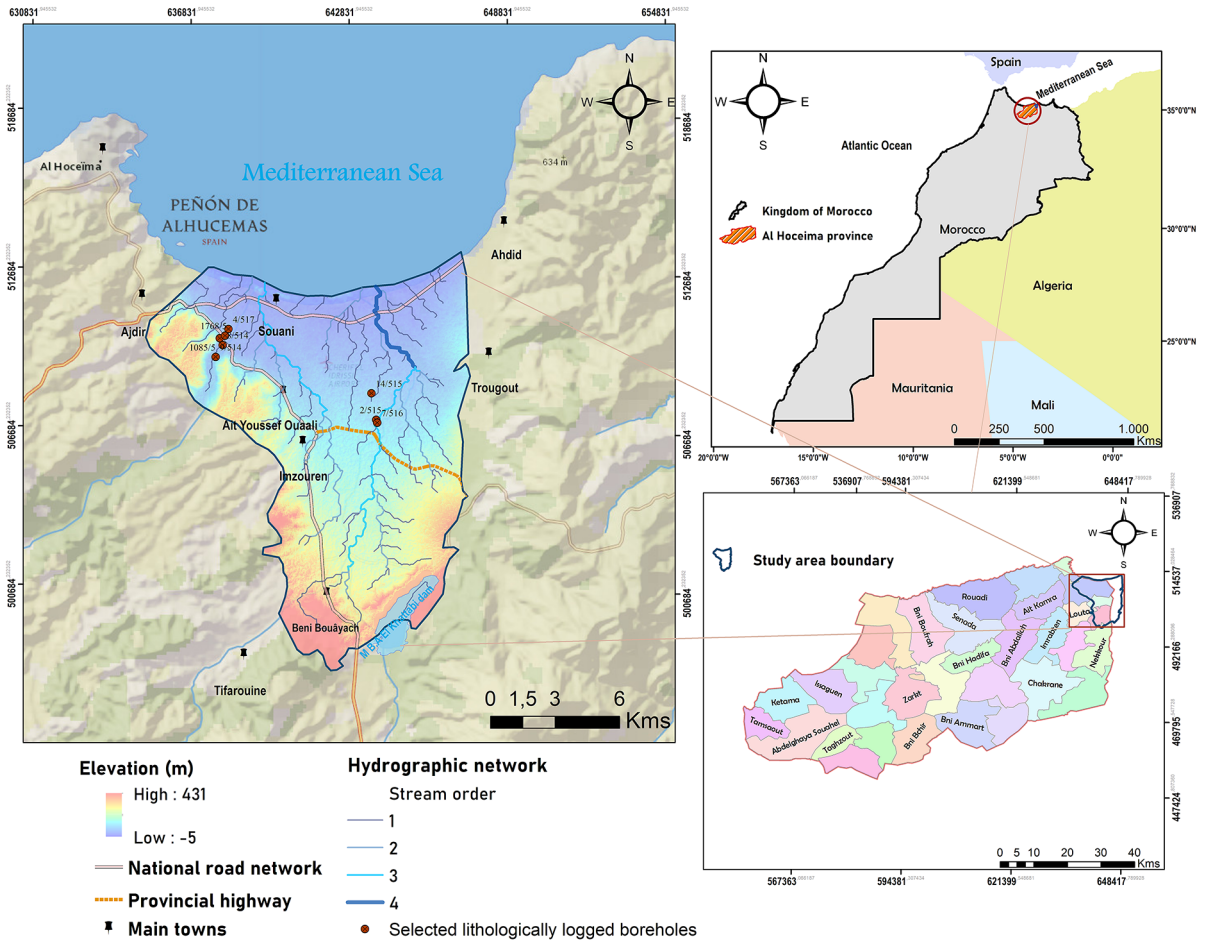

Fig. 1. Geographic location and digital elevation map of the study area

subjected to recurrent earthquakes induced by the presence of active thrust faults observed eastward near the coastline (Trougout fault) and westward (Imzouren-Ajdir fault) (Adimalla, 2020). This seismogenic source, notably Trougout fault, gives way to a local intrusion of Mediterranean seawater which borders the northern part of the study area, therefore inducing groundwater depletion (Armugha Khan, 2020).

The catchment area is flat to nearly flat with topographic elevations ranging from -5 in the northern coastal corner to 431 meters with respect to the mean sea level, found in the southwestern portion. The terrain is characterized by gently sloping topography with an average soil slope of 1% (El Hammoudani et al., 2020, El Hammoudani, 2021, Bouhout et al., 2022). The studied area is dominated by a typically Mediterranean semi-arid climate. The yearly average precipitation in the area is around 350 mm irregularly distributed across space and time, whereas the mean potential evapotranspiration rate value, estimated by (Benabdelouahab, 2019), is higher than 1700 mm per year. The latter value largely exceeds the annual rainfall received across the basin. The mean monthly temperature is quite stable and oscillates around the annual average temperature of 18°C. According to (Bouhout et al., 2023), the coastal fringe is characterized by higher humidity and temperatures but receives lower amount of rainfall.

Geological and hydrogeological background

The tectonic depression, generated by a collapse event, led to the formation of the Ghiss-Nekor valley. The study area is commonly bordered by shale-sandstone flysch formations, apart from the northwestern and northeastern boundaries marked by the presence of limestones and Plio-Quaternary vulcanites, respectively. Additionally, coalescing alluvial fans were developed at the eastern boundary, the most significant among them being located in the southeast along the main inflowing tributaries of Nekor River (Benabdelouahab et al., 2019). The sedimentary sequence deposited in the investigated plain is comprised of thick Plio-Quaternary units including sand, pebble, and gravel sometimes intercalated with silty-clayey layers. The latter geologic entities, extending in the subsurface, constitute

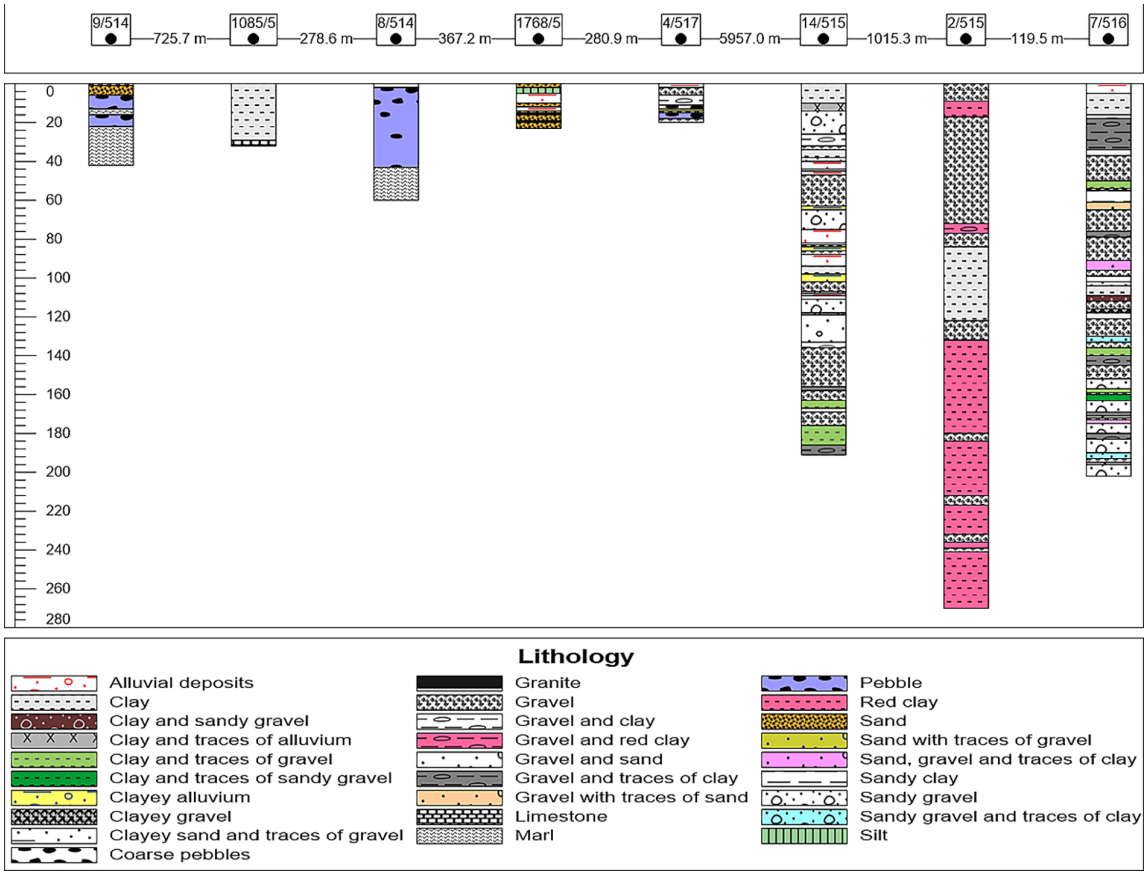

Fig. 2. Borehole logs reflecting lithological composition within the study area

the unconfined alluvial Ghiss-Nekor aquifer. Examination of the available lithological logs for 8 selected boreholes (Fig. 2) showed heterogeneous lithological classes including alluvial gravel, sand and pebbles with alternations of clay bands and silt layers reflecting a semi-pervious condition. Marls and thin limestone layers are also underlying some locations along the Ghiss river.

According to (Salhi, 2008) the thickness of water-bearing alluvium increases to a maximum of 430 meters at two local depressions near Imzouren town and Souani Beach containing the most permeable units. Furthermore, the central west and northwestern portions are characterized by the highest transmissivities (values ranging between 2×10^{-2} and 6.4×10^{-2} m²/s) (Bouhout et al., 2022, Bouhout et al., 2023). Transmissivity is a crucial variable controlling groundwater salinity; the highly transmissive thick formations enable a faster groundwater flow, therefore leading to the dilution of the groundwater through rapid infiltration of higher amount of low-salinity freshwater (Aghazadeh, 2010, Ferchichi, 2018, Purwoarminta, 2018). The phreatic conditions are emphasized by the storativity values varying between 2.2% and 5.3%, around an average of 4%. The aquifer is mainly recharged by percolation of precipitation, direct infiltration of river water (the Nekor and Ghiss major rivers) as well as from irrigation returns.

Data sources and processing

The quality of groundwater was evaluated based on the secondary groundwater quality data obtained from the databases managed by the National Office of Electricity and Drinking Water (ONEP) and Loukkos Hydraulic Basin Agency (ABHL). In total, 13 boreholes were selected from the database of drinking-water pumping boreholes, maintained by the ONEP, given the availability and adequacy of their water-quality data including 21 physical and chemical parameters. The quantification of groundwater quality index (GWQI) and SPI was conducted using the analytical results derived from these boreholes (collected on wet season of December 2019) sampled periodically by the National Office of Electricity and Drinking Water. It is worth noting that the public supply wells are characterized by longer depth and screens, and they are pumped at significantly higher rates, compared to private wells; thereby they produce representative groundwater samples (Kelly and Wilson 2008). It is also worth mentioning that the groundwater samples were collected and analyzed by the expert staff within the water management organisations (ABHL and ONEP) in accordance with standard analytical procedures for assessing water quality. The lists available at ONEP (2021) – section 5 and section 7 – (Rodier, 2009) describe the approved sampling protocols and analytical procedures. These various methods and instruments are summarized below. Measurement of physical and chemical characteristics (such as pH, turbidity, dissolved oxygen (DO), Electrical conductivity (EC), Oxidation-Reduction Potential (Eh)) was carried out in-situ using calibrated portable multi-parameter and handheld turbidimeter devices. The calcium concentrations and total hardness were estimated using the EDTA titration method. The contents of Na^+ and K^+ were determined by Atomic Absorption Spectrometry (AAS). Ion chromatography was applied for the quantification of major anions, while the concentration of Nitrate ions was measured with a Skalar continuous flow analyzer. Boron concentrations were analyzed by means of the Molecular Absorption Spectrometry method using Azomethine-H as a reagent, and Fluoride levels were assessed by employing a potentiometric method. Quality assurance and quality control protocols consisted of blank samples and duplicates. The following equation derived by Freeze and Cherry (1979) was applied to assess the analytical accuracy by computing the ionic balance error (%IBE):

$$\%\mathrm{IBE} = \frac{\sum \text{cations} - \sum \text{anions}}{\sum \text{cations} + \sum \text{anions}} \times 100 \qquad (1)$$

where: The major ion concentrations are expressed in meq/l.

The calculated charge balance errors did not exceed the limit of ± 10% which is considered to be acceptable for the aims of this study (Kadam, 2022). The second set of qualitative data was obtained from sampling of 13 monitoring wells, performed by the Loukkos Hydraulic Basin Agency in the wet period of 2019, located across the north-central and downstream, known to be the most productive and vulnerable parts of the studied aquifer. The tools provided by ArcGIS 10.8 software package were adopted to generate the spatial distribution maps. The empirical bayesian kriging (EBK), as a geostatistical method, was applied to generate predictive maps by interpolating the values of TDS, WQI, SPI, seawater fraction and SO_4/Cl ratios. The EBK model features and its advantages were described

in detail by (Krivoruchko, 2011). This interpolation method was chosen, because it simplifies the manual aspects of creating a valid Kriging model by automatically optimizing the model parameters through an iterative process of subsetting and simulations; this approach enables to generate more plausible prediction standard errors by incorporating the uncertainty associated with the semi-variogram plotting, which is not included in the classical kriging methods. Another advantage is that the EBK yields more accurate predictions for non-stationary and small-sized datasets.

Procedure for the determination of groundwater quality index

Groundwater quality index (GWQI) was chosen as one of the effective indices to conduct preliminary characterization of the water-quality status. The particular aspect of GWQI is rating and summarizing a number of water-quality data into a single value that reveals the combined influence of the physico-chemical parameters and aims to provide straightforward and easily interpreted information (Rupias et al., 2021). Fifteen groundwater quality parameters [namely, pH, TDS, EC, Ca^{2+}, Mg^{2+}, Na^{+}, K^{+}, Cl^{-}, HCO_3^{-}, SO_4^{2-}, Boron, DO, turbidity, F^{-} and NO_3^{-}] were included in the GWQI estimation process incorporating four steps:

1. Weights allocation: weights of importance (w_i), from 1 to 5, were attributed to each of the parameters by considering its implication on the overall groundwater quality for drinking purposes. In this study, the maximum weight of 5 was assigned to basic hydrochemical parameters including dissolved oxygen, turbidity, EC, TDS, chloride, nitrate and fluoride given their higher significance in water quality assessment, whilst the less harmful remaining parameters were assigned weights between 2 and 4 according to their moderate or minor significance in water quality evaluation (Radouane et al., 2023).
2. Computation of relative weight (*Wi*): the relative weight (W_i) is calculated for each parameter using the following equation:

$$W_i = \frac{w_i}{\sum_i^n w_i} \tag{2}$$

where: W_i – the relative weight, w_i – the weight of each chemical parameter, n – the number of investigated parameters (Table 1).

3. Quality rating scale assignment: A quality rating scale Q_i was determined by applying the following equation

$$Q_i = \frac{C_i}{S_i} \times 100 \tag{3}$$

where: the rating scale (Q_i) is obtained by dividing the concentration of each chemical parameter (C_i in mg/L) by its corresponding drinking water standard according to the WHO guidelines (S_i in mg/L) and multiplying the resulting value by 100.

Quality ratings of pH and dissolved oxygen were calculated by using the following formula (Rawat et al. 2020)

$$Q_{pH,DO} = \left(\frac{C_i - V_i}{S_i - V_i}\right) \times 100 \tag{4}$$

where: V_i=7 as the ideal value for pH and 14.6 as the ideal concentration for DO.

4. Quantification of sub-indices and GWQI: The sub quality index was computed for each parameter by Equation 5:

$$SI_i = W_i \times Q_i \tag{5}$$

The resulting subindices were added together to determine the final groundwater quality index:

$$GWQI = \sum_i^n SI_i \tag{6}$$

where: SI_i is the subindex of i^{th} parameter, Q_i is the rating based on its concentration, and n is the number of parameters.

The drinking water quality was categorized, according to the obtained GWQI values, into five groups (Table 2).

Synthetic pollution index computation

As suggested by (Solangi, 2019), three steps are carried out to compute the synthetic index of pollution. The first step is to determine the constant of proportionality (K) using the following equation:

$$K = \frac{1}{\sum_{i=1}^n \frac{1}{V_S}} \tag{7}$$

where: V_s – the standard WHO level for each parameter, n – the number of parameters.

In the second step, the weight coefficient (W_i) is calculated using Equation 8:

$$W_i = \frac{K}{V_S} \tag{8}$$

Table 1. Summary of weights and relative weights assigned to the quality parameters

Parameters	WHO standards (2011)	Weight	W_i relative weight
DO	5	5	0.088
Turbidity	5	5	0.088
EC	500	5	0.088
TDS	500	5	0.088
Cl^-	250	5	0.088
HCO_3^-	120	2	0.035
SO_4^{2-}	250	4	0.070
NO_3^-	45	5	0.088
F^-	1.50	5	0.088
Ca^{2+}	75	2	0.035
Mg^{2+}	50	2	0.035
B	0.50	3	0.053
Na^+	200	3	0.053
K^+	12	2	0.035
pH	8.50	4	0.070
		$\Sigma w_i = 57$	$\Sigma W_i = 1$

In the last step, equation (10) is applied to obtain the value of the SPI:

$$SPI=\sum_{i=1}^{n}\frac{V_0}{V_S}\times W_i \quad (9)$$

where: V_0 – the observed concentration for the *i-th* water quality parameter.

In this study, the abovementioned procedure was applied to the same water-quality parameters that were adopted for estimating the GWQI. Saltwater fraction as a tool for quantifying the contribution of saline encroachment The proportion of seawater in a particular groundwater sample is often obtained mathematically based on the conservative mass balance equation as follows:

$$f_{seawater}=\frac{(C_{Cl^-,sample}-C_{Cl^-,freshwater})}{(C_{Cl^-,seawater}-C_{Cl^-,freshwater})} \quad (10)$$

where: $f_{seawater}$ is the proportion of seawater, C_{Cl^-} (meq/l) is the Cl^- content of the groundwater sample, $C_{cl^-,freshwater}$ (meq/l) and $C_{cl^-,seawater}$ (meq/l) represent the concentrations of Cl^- ions in the freshwater and marine water end members, respectively.

Chloride concentration was employed as a tracer to compute the theoretical mixing ratios of freshwater-seawater given its conservative properties as it does not co-precipitate or interact with other ions. In this study, a sample collected during the monitoring campaign carried out in 2011 by the ABHL is considered to be representative of freshwater end member. This sample, with baseline chloride concentration of 142 mg/L, is obtained from the northwestern part of the plain which is a potential groundwater recharge zone and it was selected given its low electrical conductivity as well as near neutral pH. The average chloride content of local seawater samples, collected by experts of the ONEP at five beach wells intake sites supplying seawater desalination facility along Sfiha Beach, was regarded as the seawater end member ($C_{Cl^-,seawater}$=19860 mg/L). On the basis of the calculated percentages of seawater, the theoretical concentration $C_{i,mix}$ of an ion i associated with conservative mixing of seawater and freshwater can be estimated from Equation 7:

Table 2. Groundwater quality categories based on the WQI value

Ranges of GWQI	Water quality status
<50	Excellent water
50–100	Good water
100–200	Poor water
200–300	Very poor water
>300	Water unfit for drinking purpose

$$C_{i,mix}=f_{seawater}\times C_{i,seawater}+(1-f_{seawater})\times C_{i,freshwater} \quad (11)$$

where: $C_{i,seawater}$ – the concentration of the ion in seawater, $C_{i,freshwater}$ the concentration of the ion in freshwater (in milli-equivalents per liter) and $f_{seatwer}$ the percentage of seawater. For each ion i, the difference between the observed concentrations and the theoretical concentrations resulting from conservative mixing is known as ionic delta and is inferred using the following equation:

$$\Delta C_i=C_{i,sample}-C_{i,mix} \quad (12)$$

Ionic delta (Δ) is widely implemented to delineate the geochemical reactions occurring between the solid and liquid phase in coastal aquifers leading to deviations from the simply mixed composition (Abu-Alnaeem et al., 2018). Negative and positive values of ionic deltas reflect that there is a deficiency or an enrichment of this ion concentration in groundwater sample, respectively, compared to theoretical mixing. In turn, near-zero values suggest that the ion content is derived from conservative mixing (Abu-Alnaeem et al., 2018).

RESULTS AND DISCUSSION

Tables 3 and 4 summarize the descriptive statistics of the groundwater quality dataset along with the number of groundwater samples reaching concentrations of the investigated water quality parameters beyond the national and World Health Organization guideline values.

General physicochemical parameters

The groundwater samples are neutral to slightly alkaline with a pH range of 7–7.31 and a mean value of 7.1. All pH values corresponding to the investigated water samples are within the permissible range prescribed by the WHO and Moroccan standards (6.5–8.5) for domestic water supply which does not reveal extremely acidic nor basic conditions.

The highest pH values coincide with lower groundwater temperature. Redox potential values ranged from 166 to 183 mV, with an average value of 174 mV; thus, it was inferred that oxidizing nature prevails within this alluvial aquifer. The highest value could be attributed to the infiltration of oxygen-enriched water and the existence of redox-active salts and minerals. The dissolved oxygen (DO) contents were in the range of 5–9.9 mg/L with an average of 7.05 mg/L; therefore, all the extracted samples are oxygenated and the DO values remained higher than the minimum standard value recommended for drinking water. This aerobic feature could be triggered due to additional dissolved oxygen brought through extensive groundwater abstraction and to the prevalence of shallow unconfined conditions exposing groundwater to interact with atmospheric oxygen. These conditions also promote the occurrence of nitrification process (Bodrud-Doza, 2019).

The turbidity of the investigated samples varied between 0.17 and 2 NTU (average=0.53). 92% of the samples exhibited turbidity values below 1 NTU, while the WHO and the national standard permissible level is 5 NTU. The highest turbidity value of 2 NTU was observed in the sample collected 1 kilometer North of Beni Bouayach given the contribution of suspended particles carried into the well due to the steep hydraulic gradient. The lower turbidity values are indicative of the proper construction and installation of the wells (Jha, 2020, Yifru, 2020).

Table 3. Statistical summary of hydrochemical constituents of samples from ONEP wellfield

Parameters	Minimum	Maximum	Average	Std. deviation	Coefficient of variation
pH	7	7.31	7.10	0.10	0.01
Temperature(°C)	18.5	22	20.42	1.17	0.06
Eh (mV)	166	183	174	4.76	0.03
DO (mg O_2/L)	5	9.9	7.05	1.55	0.22
Turbidity(NTU)	0.17	2	0.53	0.49	0.92
EC (µS/cm)	2430	4790	2986.15	628.79	0.21
TDS (mg/L)	1555.2	3065.6	1911.14	402.42	0.21
TH (mg/L)	268.25	445.05	352	49.38	0.14
Ca^{2+} (mg/L)	196	314	236.92	36.55	0.15
Mg^{2+} (mg/L)	66.25	147.85	115.08	21.70	0.19
Cl^- (mg/L)	408	1350	588.62	248.55	0.42
SO_4^{2-} (mg/L)	551	803	628.85	78.80	0.13
HCO_3^- (mg/L)	268.4	451.4	340.19	46.90	0.14
NO_3^- (mg/L)	3.42	88	19.45	22.27	1.15
F^- (mg/L)	0.21	0.39	0.27	0.05	0.16
SiO_3^{2-}(mg/L)	11	20	15.62	2.57	0.16
NH^{4+} (mg/L)	0	0.05	0.01	0.02	1.49
Fe^{2+} (mg/L)	0	0.02	0	0.01	2.60
B (mg/L)	0.17	0.65	0.30	0.12	0.40
Na^+ (mg/L)	138.85	684.99	349.85	130.94	0.37
K^+ (mg/L)	1.9	7.2	4.07	1.64	0.40

Table 4. The percentage of unsuitable samples exceeding Moroccan standards and the maximum permissible limits prescribed by WHO for domestic purposes

Parameters	WHO standards (2017)	Moroccan standards	Samples exceeding WHO standards	Samples exceeding Moroccan standards
pH	6.5–8.5	6.5–8.5	0	0
DO	5	>5 mg/L	12 (92.3%)	12 (92.3%)
Turbidity	5	5	0	0
EC	1500	2700	13 (100%)	7 (53.8%)
TDS	500–1500	–	13 (100%)	–
Cl^-	250–600	750	3 (23%)	1 (7.69%)
HCO_3^-	300	–	12 (92.3)	–
SO_4^{2-}	400	200–400	13 (100%)	13
NO_3^-	50	50	1 (7.69%)	1 (7.69%)
F^-	1.50	1.50	0	0
SiO_3^{2-}	100	100	0	0
TH	100–500	300	0	12 (92.3%)
Ca^{2+}	75–200	100	12 (92.3%)	13
Mg^{2+}	50–150	100	0	11 (84.61%)
B	0.5	0.3	1 (7.69%)	5 (38.46%)
NH^+_4	0.2	0.5	0	0
Fe^{2+}	0.3	0.3	0	0
Na^+	200	–	11 (84.6%)	–
K^+	12	–	0	–

Impact of land use/land cover on the chemical characteristics of groundwater

Land use and land cover correspond to two distinct concepts; land cover designates the natural envelope including forests, wetlands, and water bodies. Land-use represents human activities and settlements, related to industrialization/urbanization found over land surfaces (Zghibi, 2016). The land use map of the study area (Fig. 3) was derived using land use/land cover layers from 10 m resolution Sentinel-2 time series (2017–2021) available through the Esri's Living Atlas data portal. The major portion of the eastern and central parts of the study area comprises agricultural crops and rangeland land cover features, while the dominant land-use includes built-up area, occupying most of northern and western portions. The electrical conductivity contour lines, superimposed on the produced land-use map, illustrated that low groundwater quality regions are located within zones subjected to multiple polluting anthropogenic activities identified in the study area. Electrical conductivity of the Ghiss-Nekor groundwater exhibited an increasing trend as distance to the wastewater treatment plant decreases; as displayed by the closely-spaced simulated electrical conductivity contour lines. This result is in accordance with the recent findings of (Bourjila, 2021) who detected highly mineralized groundwater downstream of the water treatment plant which could be justified by the infiltration of wastewater from this treatment facility. A similar trend was found in the vicinity of the coastal touristic site near Souani (EC > 6000 µS/cm). Also, a localized rise in electrical conductivity was found close to the uncontrolled landfill site located in a dry riverbed section of Oued Nekor, northeast of Beni Bouayach town. This likely reflects the impact of percolating leachates, emanating from the landfill, on the underlying groundwater quality. Moreover, a desalination plant, commissioned in December 2019, was installed to meet the rising freshwater demands across the study area. The environmental and hydrologic disturbance was minimized since the seawater intake structure (beach wells) was drilled underground and the seawater desalination plant was set up near water distribution networks and close to the Mediterranean Sea to reduce pumping pipeline and land-use required for the water distribution system (ONEP 2020). As reported, the presence of multiple gasoline stations within the considered study area constitutes

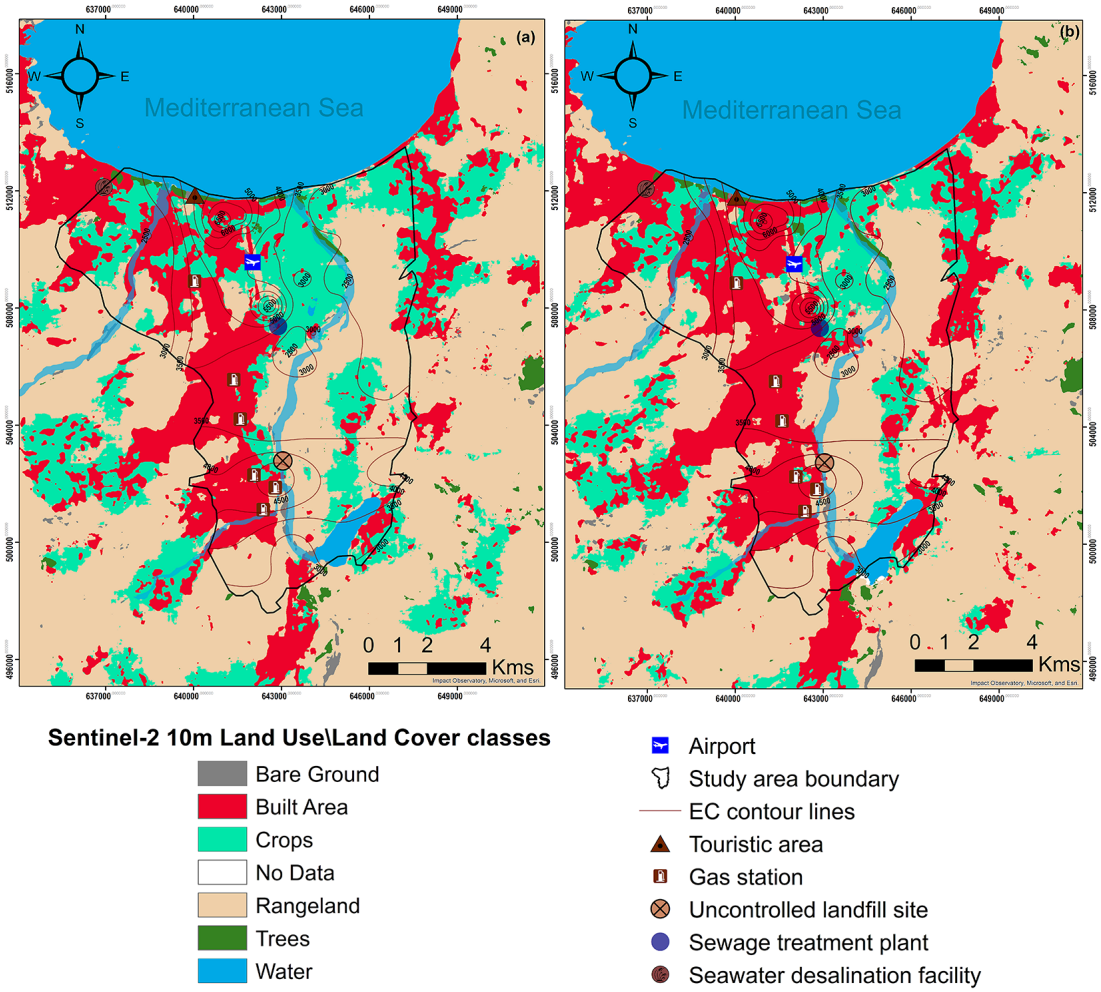

Fig. 3. (a) Overlay of electrical conductivity contours and land use map for the year 2017, (b) Land use map for 2021

Table 5. Groundwater classification based on electrical conductivity

EC (µS/cm)	Enrichment of salts	Groundwater quality status
<1500	Low salinity	Desirable to permissible
1500–3000	Medium salinity	Not permissible condition
>3000	High salinity	Low and hazardous

another significant factor contributing to groundwater pollution.

Classification of groundwater based on salinity level (EC and TDS)

Electrical conductivity is an essential indicator quantifying the amount of mineral or chemical ionic substances dissolved in the groundwater which makes the solution conductive, and categorizing each sample in terms of their salinity level and suitability for various purposes (Shukla, 2017). The values of electrical conductivity recorded in the sampled wells lie between 2430 and 4790 µS/cm with a mean value of 2986.15 µS/cm. Referring to the categorization proposed (Table 5), 61.5% of the groundwater samples are characterized by medium salts enrichment, while high level of salt enrichment is prevalent in 38.5% of the samples classified as hazardous for consumption. None of the samples fell within the permissible category (EC < 1500 µS/cm). Electrical conductivity (EC) measurements have been commonly used to compute the amount of total dissolved solids (TDS). Hem (1985) derived the following empirical relationship between EC and TDS:

$$TDS\ \left(\frac{\text{mg}}{\text{L}}\right) = k\ \times EC(\frac{\mu S}{cm}) \qquad (13)$$

where: k – a correlation factor found within the range of 0.55–0.75.

In this research, EC was converted to TDS content by multiplying the EC values by the average (k=0,64) over the range of conversion factors. Several research studies approved the selection of 0.64 as a multiplying factor to infer dissolved-solids concentration from the measured EC, within the range of 100–5000 µS/cm. The TDS values obtained at the wells monitored by the National Office of Drinking Water (ONEP Co.) were in the range of 1555.2–3065.6 mg/L (mean level of 1911.14 mg/L). Comparison of the TDS values with the classification established by Freeze and Cherry (1979) (Table 6) reveals that all the groundwater samples belong to the brackish category. As per the TDS classification categories (Table 6), 92.3% of the set of samples are listed as being suitable for agricultural purposes, except one sampled site where groundwater is found to be unfit for consumption and irrigation uses. Thus, a prior treatment is required before direct consumption of such highly mineralized waters.

The additional qualitative data associated with the wells monitored by the ABHL enabled us to generate the spatial distribution map of TDS. Elevated TDS values are found in the northern coastal fringe few kilometers southeast of Souani beach (Fig. 4), as a consequence of heavy groundwater pumping carried out to supply water for beach shower and local coffeeshops/restaurants. The occurrence of high TDS concentration near the coast is due to the process of freshwater-seawater mixing resulting in the supply of marine-derived ions to the groundwater. This phenomenon is favored by the accumulation of thick sequence of highly permeable Quaternary sediments forming a significant water-bearing horizon near the Souani beach. Moreover, two isolated salinized zones (TDS > 3000 mg/L) are observed: the first is located at about 2 kilometers north-east of Imzouren town, the second at 1 kilometer North of Beni Bouayach town; the high TDS values in these inland areas could be related to prevailing anthropogenic inputs from agriculture, domestic effluents and industrial activities (proximity to the industrial unit and the wastewater plant of Imzouren, and the uncontrolled landfill). The TDS content is relatively lower in the North-western, North-eastern and central parts of the study area given the contribution of freshening process favored through local recharge from the Nekor and Ghiss rivers and the eastern alluvial fan (Fig. 5).

Table 6. Classification of groundwater based on TDS

TDS (mg/L) Freeze and Cherry (1979)	Classification
TDS < 1000	Freshwater
1000 < TDS ≤ 10000	Brackish water
10000 < TDS ≤ 100000	Saline water
TDS ≥ 100,000	Briny water
TDS (mg/L) Davis and DeWiest (1966)	Suitability for purposes
TDS < 500	Desirable for drinking
500 < TDS < 1000	Permissible for drinking
1000 < TDS < 3000	Useful for irrigation
TDS > 3000	Unsuitable for drinking and irrigation

Trends of major ionic components

The amount and sequence of the main cations and anions dominating the groundwater chemical composition can be employed to examine the alteration of groundwater quality throughout the study area. The chloride ion content varies from 408 to 1350 mg/L with an average value of 588.62 mg/L. Chloride content of all the samples was detected at concentrations above the allowable limit (250 mg/L), prescribed by the WHO. The elevated concentration of Chloride could be derived from multiple sources such as the dissolution of evaporites, mixing with seawater or sewage, and the effects of irrigation return flow (Armugha Khan et al., 2020).

The sulfate (SO_4^{2-}) concentrations in the samples, ranging from 551 to 803 mg/L and a mean value of 628.85 mg/L, exceeded the WHO maximum permissible limit for drinking water in all the investigated wells. The excessive amount of SO_4^{2-} can arise naturally from dissolution and leaching of sulfate minerals, or the possible leakage of agrochemicals from agricultural activities. High values of SO_4^{2-} content could also reflect the effect of seawater influx; because a proportion of only 3% of seawater mixed with freshwater would raise the sulfate levels released in groundwater by approximately 80 mg/L. The range of HCO_3^- concentrations in the sampled locations lies between 268.4 and 451.4 mg/L (average concentration of 340.19 mg/L). The HCO_3^- values from more

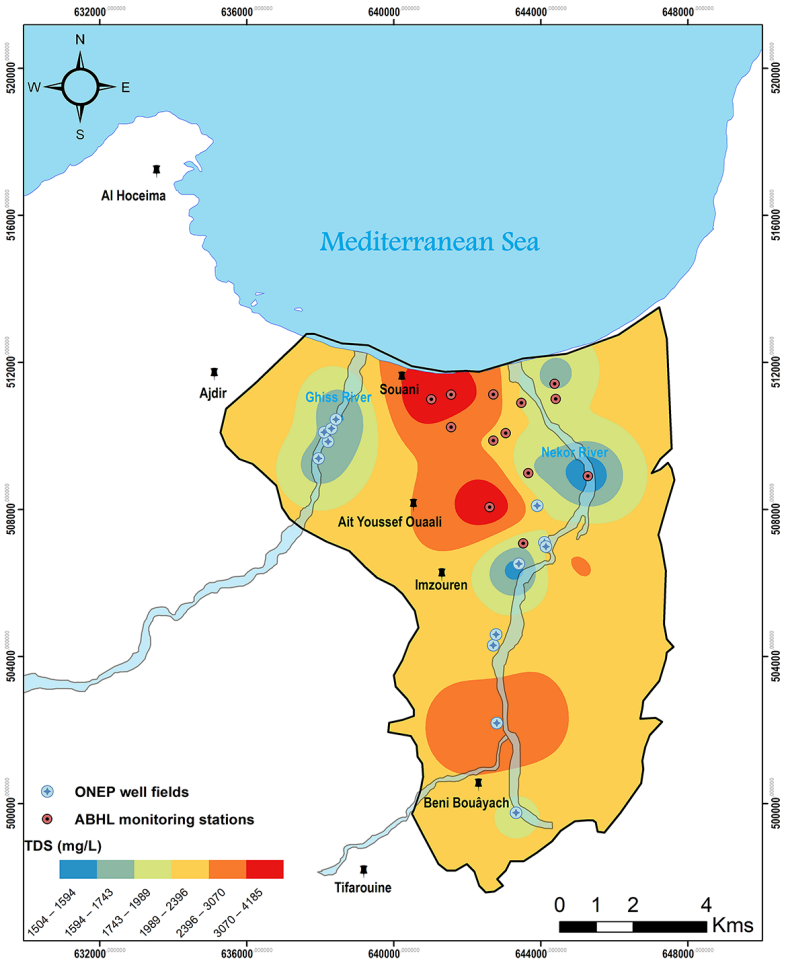

Fig. 4. Distribution of TDS in the study area

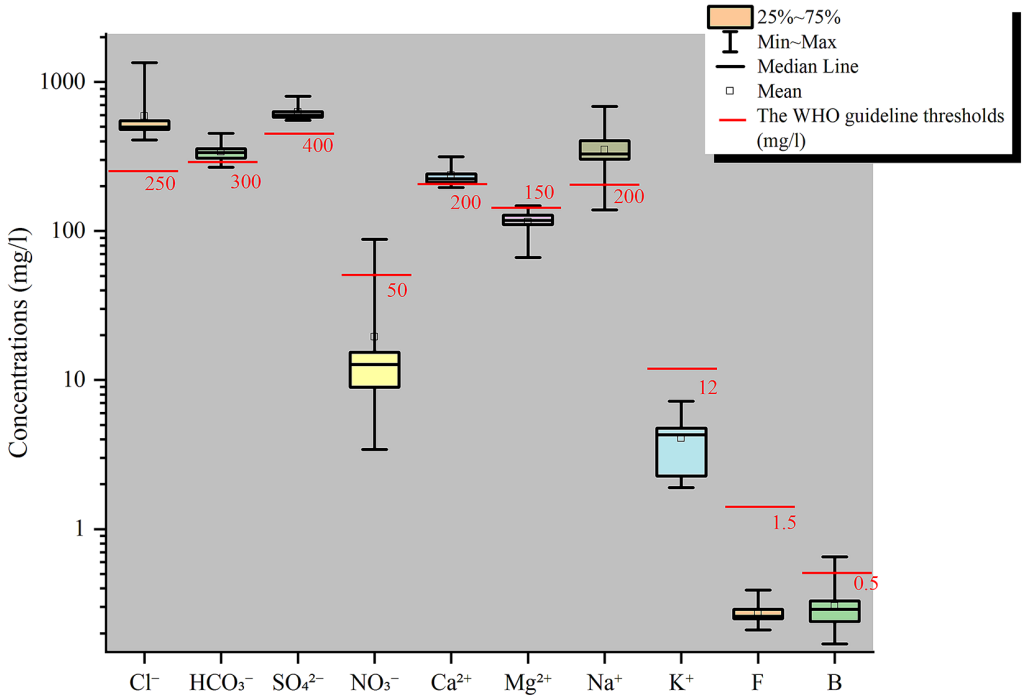

Fig. 5. Box and whisker plot of major ions in the Ghiss-Nekor aquifer, illustrating basic statistics compared with WHO thresholds

than 90% of the samples are beyond the permissible WHO standards (200 mg/L). Enrichment of HCO_3^- ions, as the main components of alkalinity in groundwater, results primarily from the dissolution of carbonate precipitates – such as calcite and dolomite- and secondarily from the decomposition of atmospheric CO_2 gas and anoxic biodegradation of organic matter. The NO_3^- concentrations indicate a wide variation, ranging from 3.42 to 88 mg/L. There is only one sample with concentration falling beyond the WHO permissible limit. Human activities and intensive agriculture-related practices are common sources for occurrence of elevated concentration of nitrates due to the generation of nitrogenous organic matter from chemical fertilizers and domestic waste (Ayyandurai, 2022).Respective concentrations of fluoride (F^-) and boron (B) were in the range of 0.21–0.39 mg/L and 0.17–0.65. The comparison of fluoride concentrations with the safe level (1.5 mg/L) recommended by the WHO reveals that all the groundwater samples are within the prescribed range of suitability regarding fluoride content. In turn, the maximum permissible limit set by the Moroccan standards for boron concentration is exceeded at 5 wells. The release of fluoride ions could derive from weathering of fluoride-rich minerals (limestones and dolomite), occurrence of high evapotranspiration level and the long residence time of waters in the subsurface. As reported in several case studies conducted in the Mediterranean basin, the presence of boron in groundwater might arise naturally from evaporitic deposits, water-rock interaction and mixing with seawater or from contamination by human activities releasing varied products containing boron; such as fertilizers, pesticides and detergents found in domestic wastewater and industrial effluents.

The silicate concentrations in groundwater of the study area vary between 11 and 20 mg/l with an average of 15.62 mg/L. The input of silicate is affected by agricultural and domestic wastewater or chemical weathering of silicate minerals along with leaching of fluoride (Errahmouni, 2017, Ghalit et al., 2017). The range of Calcium concentrations varies over the study area from 196 to 314 mg/L with an average of 236.92 mg/L. Over 90% of the groundwater samples contained the calcium concentrations exceeding the WHO threshold value. The common contributors to Ca^{2+} enrichment include the weathering process of precipitated carbonate minerals (calcite and dolomite) during aquifer recharge, possible input of gypsum used for agricultural activities or the occurrence of reverse cation exchange (Errahmouni, 2022). The majority of samples exhibited the magnesium concentrations (between 66 and 148 mg/l) below the WHO maximum permissible limit for drinking water (<150 mg/l). The dissolution of limestone, influence of the marine environment and ion exchange could be responsible sources for the increase of magnesium in coastal groundwater, while the abundance of Ca^{2+} over Mg^{2+} might indicate a slower weathering of magnesium bearing minerals. The hardness of water is related to the level of calcium and magnesium cations in the groundwater samples.

The sodium concentration attains 685 mg/L with a minimum value of about 139 mg/L. Only two samples fell below the WHO permissible limit (200 mg/L). Sodium enrichment in groundwater is related to the vicinity of industrial zones, evapotranspiration, exposure to seawater intrusion, or chemical weathering of evaporites at the inland sites (Mukate et al. 2019; Nouayti et al. 2022). The studied samples are of good quality regarding potassium ion (1.9–7.2 mg/L); none of the observations surpassed the WHO threshold of 12 mg/L.

Graphical representation of hydrochemical facies

The Piper trilinear diagram is an effective graphical approach to infer prominent groundwater chemical facies by plotting the concentrations of major constituents in two ternary diagrams representing cations and anions, each parameter is then projected in a diamond shaped field. The hydrochemical facies types are governed by various processes such as the lithological characteristics, flow pattern of the aquifer and the residence time. As shown in the cations ternary plot (Fig. 6), the majority of samples belong to the no dominant pole except for one well (P7) that fell in the sodium type. Concerning the anion facies, it was noticed that 3 groundwater samples were projected towards the chloride type, while the remaining 77% of samples fell in the no dominant class with a tendency to the sulfate type. The central rhombus-shaped plot revealed the dominance of mixed Ca-Mg-Cl water type, while 15% of the samples (from locations P3 and P4) were found in Ca-Cl facies type and one sample (P7) belonged to Na-Cl-SO_4 chemical facies.

The Ca-Cl and Na-Cl-SO_4 types reflect respectively the contribution of reverse

ion-exchanged waters and the effect of leaching of evaporates in addition to septic tank effluents as well as leachate seepage given the proximity to the uncontrolled landfill (for location P7) (Benabdelouahab et al., 2019). The samples characterized by Ca–Cl type water may also be located at a leading edge of the seawater plume. In turn, the abundance of mixed Ca-Mg-Cl water type could be derived from the processes of ion-exchange reaction and water-rock interaction. Moreover, the Piper diagram illustrates the dominance of strong acidic anions over weak acids ($Cl+SO_4>HCO_3$).

However, the sole dependence on Piper plots is not sufficient to identify the facies evolution sequence during freshening and salinization phases (Ghiglieri et al. 2012). Therefore, based on the Hydrochemical Facies Evolution Diagram (HFE-D), more information regarding the rate of groundwater quality recovery across coastal environments was revealed. In the conducted study, as shown in Figure 7, five hydrochemical facies were identified; MixNa-MixCl (38.4%), MixNa-MixSO_4 (23.1%), MixCa-MixCl (15.38%), MixNa-Cl (15.38%) and Na-Cl (7.7%). Three samples (locations P8, P10, P12), corresponding to the freshening phase with MixNa-MixSO_4 facies, delineated the contribution of groundwater recharge that took place from the Nekor river enriched with Sulfate along with leaching of gypsum beds associated with Triassic formations (Benabdelouahab et al., 2019). Some groundwater samples (sites P6, P7, P9, P11, P13), despite being located far enough from the coast, were placed within the encroachment phase and characterized by mixed hydrochemical types, i.e. a sequence of mixNa-mixCl, mixNa-Cl and Na-Cl facies.

This observation implies that NaCl inputs were released into these upstream sampling sites through septic tank waste infiltration, localized weathering of evaporitic salts given the extended water-rock interaction, along with evaporation. The majority of points sampled over the northwestern part fell in the MixNa-MixCl facies except for two samples belonging to MixCa-MixCl water facies which illustrates reverse ion exchange process favored by the presence of clay particles within the aquifer matrix. Moreover, the sampling site P1, located close to the coastal fringe, corresponds to the freshening field characterized in this case by MixNa-MixCl facies.

Water-rock interactions: cation-exchange processes

The chloro-alkaline indices (CAI1 and CAI2) are simple indicators depicting the types of ion-exchange processes occurring between the groundwater and its host environment.

The positive and negative CAI values suggest the induction of reverse ion exchange and direct ion exchange, respectively. In the present study, the calculated CAI_1 and CAI_2 were positive in 53.84% of the groundwater samples (Fig. 8) which implies the occurrence of reverse ion exchange reactions illustrating an exchange between Na^+ or K^+ from the groundwater with Ca or Mg of the host rock. The remaining samples illustrated a direct ion exchange, as they exhibit negative indices given the exchange of Ca^{2+} or Mg^{2+} from the water with Na^+ or K^+ in the aquifer minerals. The presence of clay particles acting as ion exchangers within the aquifer matrix induced the absorption of Na and K ion content with the simultaneous release of alkaline earth metals (Ca^{2+} and Mg^{2+}) (Gad, 2022).

Interpretation of the drinking water quality indices

Water quality index was applied to evaluate the overall groundwater suitability for drinking purpose. The water quality categories were identified based on the groundwater quality index values, ranging from 146.43 to 300.20. Around 92% of the wells are characterized by poor water quality while the groundwater sampled from one well (P7) was unfit for drinking. The interpolated map (Fig. 9a) displaying spatial distribution of the groundwater quality based on WQI estimations indicates that the WQI values were higher in the central and southern parts of the study area; this groundwater unsuitability can be attributed to anthropogenic inputs from leachates infiltration of the uncontrolled landfill, water-rock interaction and agricultural impact which induced elevated concentrations of chloride, sulfate and nitrate ions. The landfill site is located around an area covered by coarse-grained deposits characterized by high vertical permeability enhancing the percolation of the released leachate and other pollutants existing in the surface (Benabdelouahab et al., 2019). The WQI values decrease in the northwestern coastal sector which can be related to a dilution effect. The map also highlights a

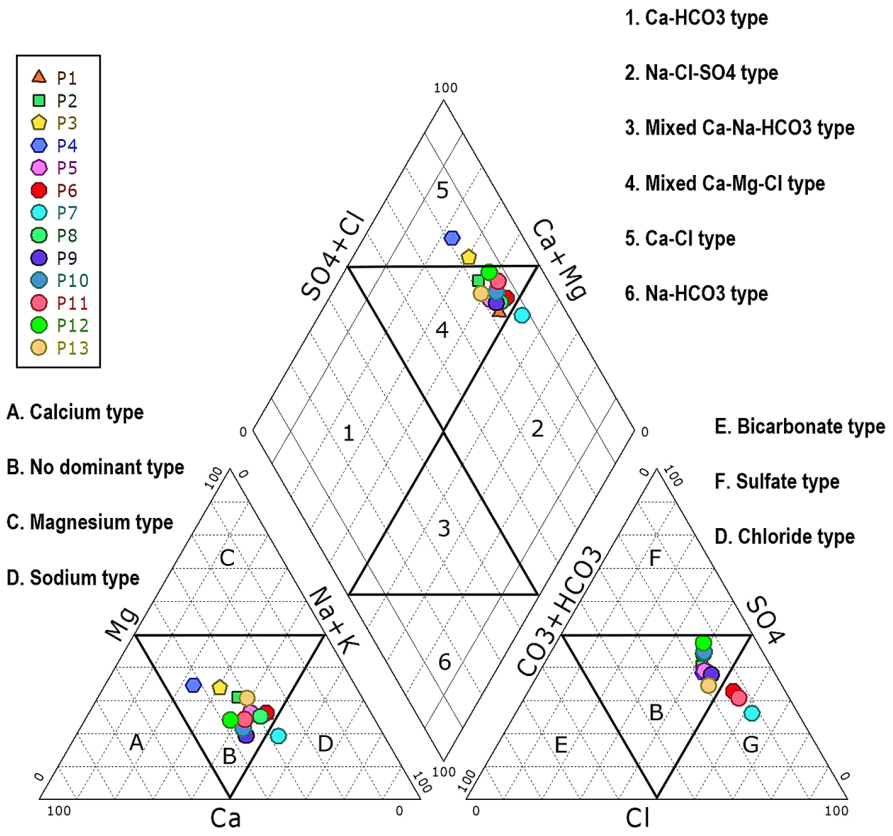

Fig. 6. Piper plot describing hydrogeochemical facies of groundwater from operating wells monitored by the ONEP

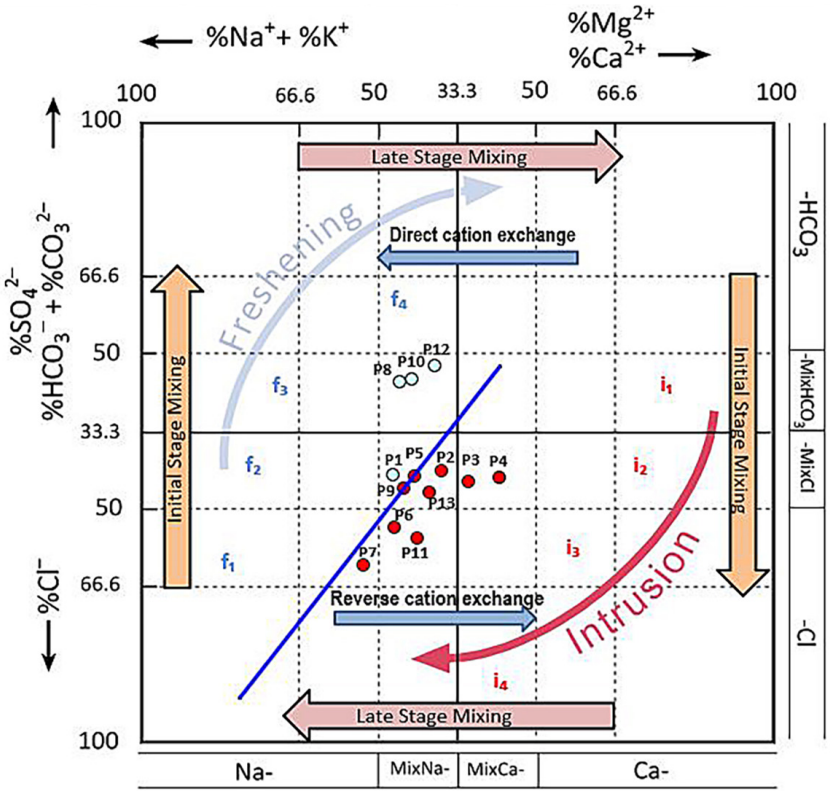

Fig. 7. Representation of the analyzed groundwater samples from ONEP wellfields on hydrochemical facies evolution diagram (HEF-D) with stages and sub-stages for salinization and freshening

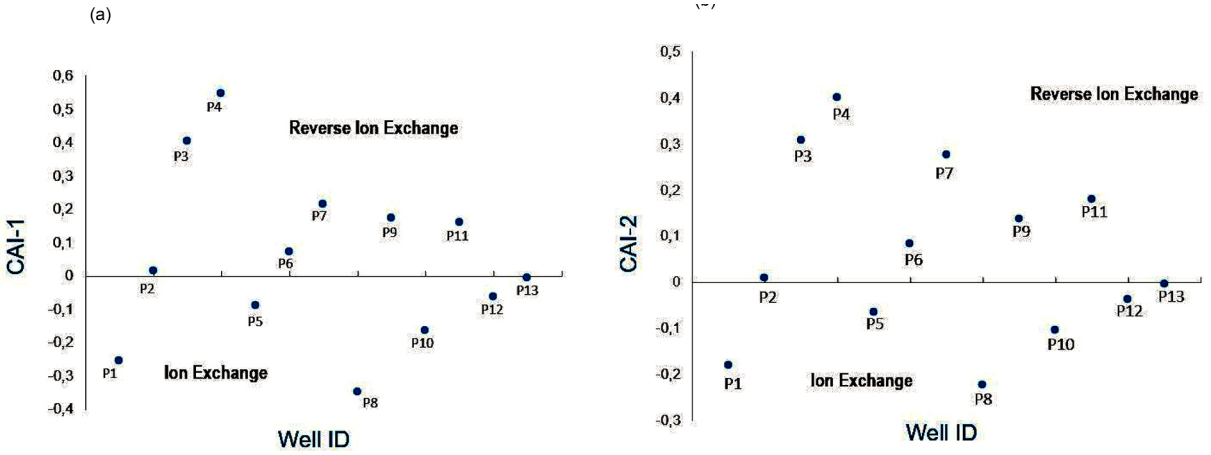

Fig. 8. Chloro-alkaline indices (CAI) (a) CAI1 and (b) CAI2 computed for groundwater samples from ONEP boreholes

pocket of the least affected groundwater restricted to a small area around the site P10 where the level of anthropogenic pollutants is lower and a slight dilution of contaminants occurs from local infiltration deriving from Oued Nekor along with lateral inflows. Thus, no sample has been categorized as adequate for direct consumption without prior treatment. The correlation matrix (Table 8) among the fifteen water quality parameters, WQI and the SPI was established to denote the effect of each water-quality parameter on the overall quality of the groundwater in the Ghiss-Nekor aquifer. Six parameters, namely TDS (r=0.94), chloride (r=0.96), nitrate (r=0.94), calcium (r=0.78), boron (r=0.82) and sodium (r=0.85) revealed a strong positive correlation with WQI values. Moreover, a moderate positive correlation was found between WQI-sulfate, and WQI and bicarbonate (r=0.53, 0.69 respectively). Therefore, it was deduced that chloride and nitrate exerted the largest impact on groundwater chemistry and quality in this alluvial plain. It is worth noting that the resulting matrix also showed the existence of a significant correlation between bicarbonate and boron contents (r=0.93), implying their common origin from the dissolution of carbonate minerals since the solubility of boron in water increases along with the CO_2 content (Salhi, 2008). Furthermore, boron is positively correlated with nitrate (r=0.83), indicating that anthropogenic nitrate sources also enhanced boron content in groundwater in the Ghiss-Nekor plain.

The resulting SPI values ranged from 0.42 to 1.04 with a mean value of 0.58. The SPI values for drinking water can be categorized into the following classes: suitable for drinking (SPI < 0.2), slightly polluted water for SPI comprised between 0.2–0.5, moderately polluted for SPI ranging between 0.5–1.0, highly polluted for SPI between 1.0–3.0, and unfit for drinking (SPI > 3.0) (Solangi et al., 2019). Accordingly, all the obtained index values exceed the minimum SPI score of 0.2 attributed to the suitable category for drinking purposes. The findings showed that groundwater is slightly polluted to moderately polluted in 38.50% and 54% of the samples, respectively. Only one sample (P7) fell under the highly polluted category. It is apparent from Fig. 9b that groundwater is relatively less polluted as one moves along the left bank of the Nekor River towards the wells located in the central portion of the basin. In addition, the spatial distribution of the SPI is roughly similar to the spatial variation observed for the WQI, particularly in the southern portion of the study area. Table 8 revealed a strong positive correlation (R=0.843) between the two scores (SPI and WQI).

Estimation of seawater intrusion contribution

The mixing rate of seawater intrusion in the investigated wells ranged between 1.3% and 6.12%; values exceeding 2% were noticed in 54% of the groundwater samples, which reflects their unreliability for human supplies. The spatially interpolated map of seawater proportion (Fig. 10), created to determine the pattern and extent of seawater intrusion in the study area, revealed a decrease of the seawater mixing ratios (<2%) in the wells located in the northwestern part of the study region despite their proximity to the shoreline; this suggests the potential role of fine-grained

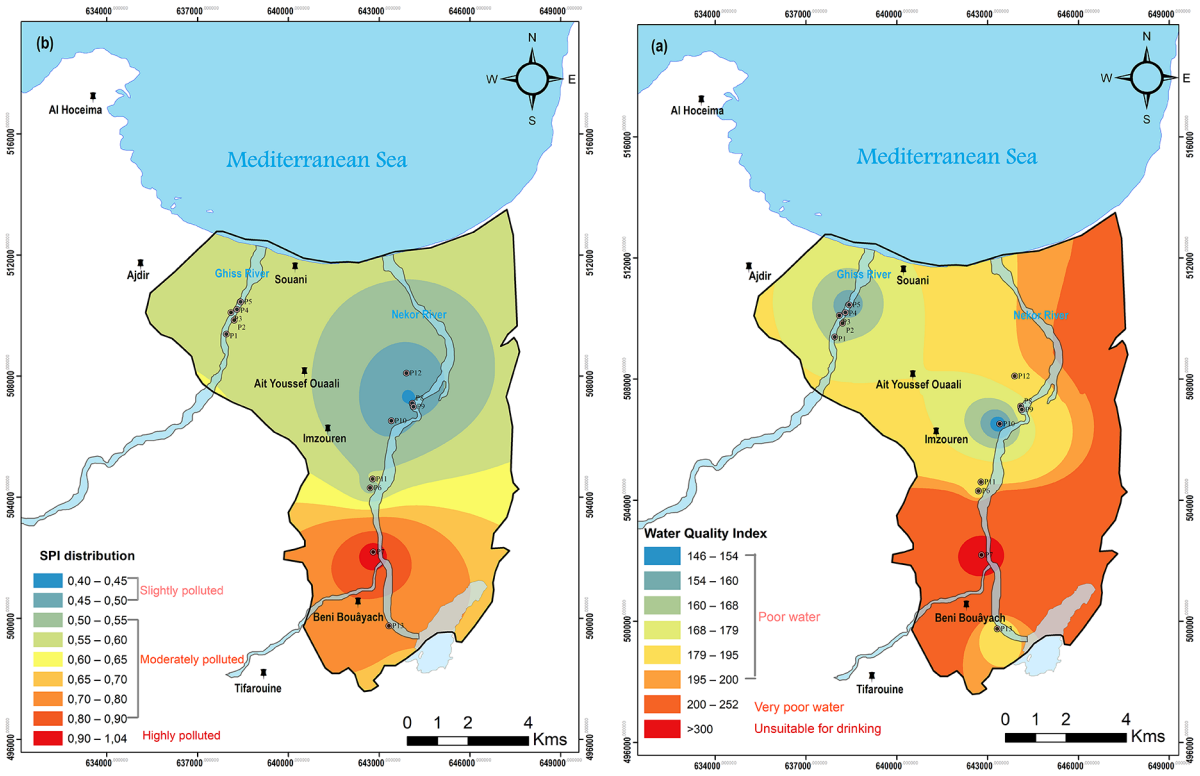

Fig. 9. Spatial distribution maps of (a) groundwater quality index and (b) synthetic pollution index in the study area

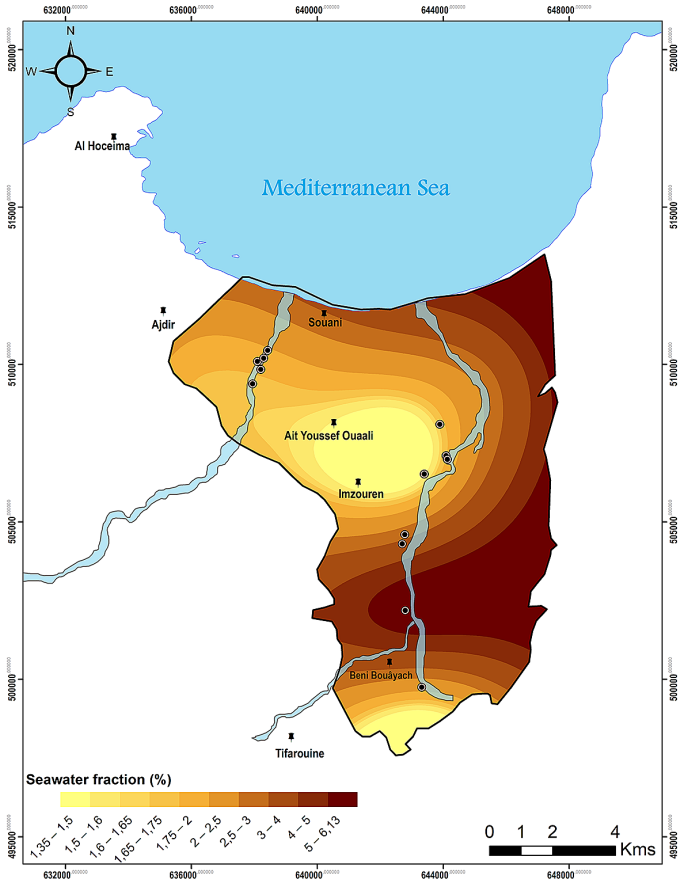

Fig. 10. Map of spatial distribution of seawater fractions along the Ghiss-Nekor aquifer

alluvium acting as a low-permeable natural barrier that restricts the intrusion of seawater and the significant water discharge of the Ghiss river serving as a hydraulic barrier that flushes the saline plume (Benabdelouahab et al., 2019). The impact of seawater decreases with increasing distance from the Mediterranean Sea coastline; however, at a few inland locations, the mixing rate of seawater intrusion was up to 4%, particularly near the uncontrolled dumpsite (east of Beni Bouayach) where the chloride level reaches 1350 mg/L.

Delineating groundwater mineralization sources

The computed SO_4^{2-}/Cl^- ratios for the unconfined aquifer of the Ghiss-Nekor basin range between 0.42 and 1.25. The SO_4^{2-}/Cl^- ratio values did not exceed the reference value of one ($SO_4^{2-}/Cl^-<1$) in 77% of the investigated samples; this highlights the excess of Cl^- over SO_4^{2-}. The SO_4^{2-}/Cl^- increases ($SO_4^{2-}/Cl^->1$) as one moves inland towards the sampling sites located on the left bank of the Nekor river, therefore reflecting the dominance of SO_4^{2-} released from weathering of sulfate-bearing evaporite minerals that prevails in the Nekor basin (Fig. 11). The highest sulfate input (at the location P12), exceeding chloride contents, could not be justified by the influence of agricultural activities since sulfate enrichment was not accompanied by high nitrate levels (Fig. 12). Interpretation of the SO_4^{2-} versus Cl^- scatterplot corroborates these findings; the samples with the highest ratio clearly diverge from the conservative mixing line between the end members – seawater and freshwater – which suggests the influx of sulfate from other sources in addition to seawater sulfate.

Examination of the NO_3/Cl^- ionic ratio

It is important to take into account the occurrence of nitrate pollution. Given the conservative

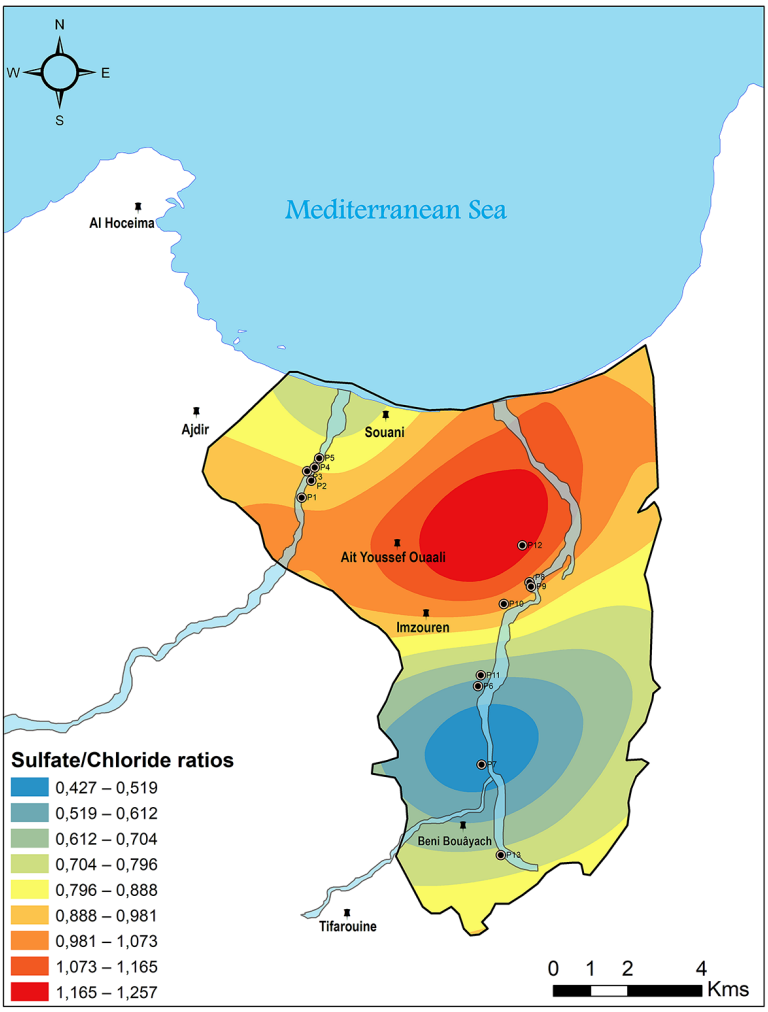

Fig. 11. Spatial variation of SO_4/Cl ionic ratio in the Ghiss-Nekor aquifer

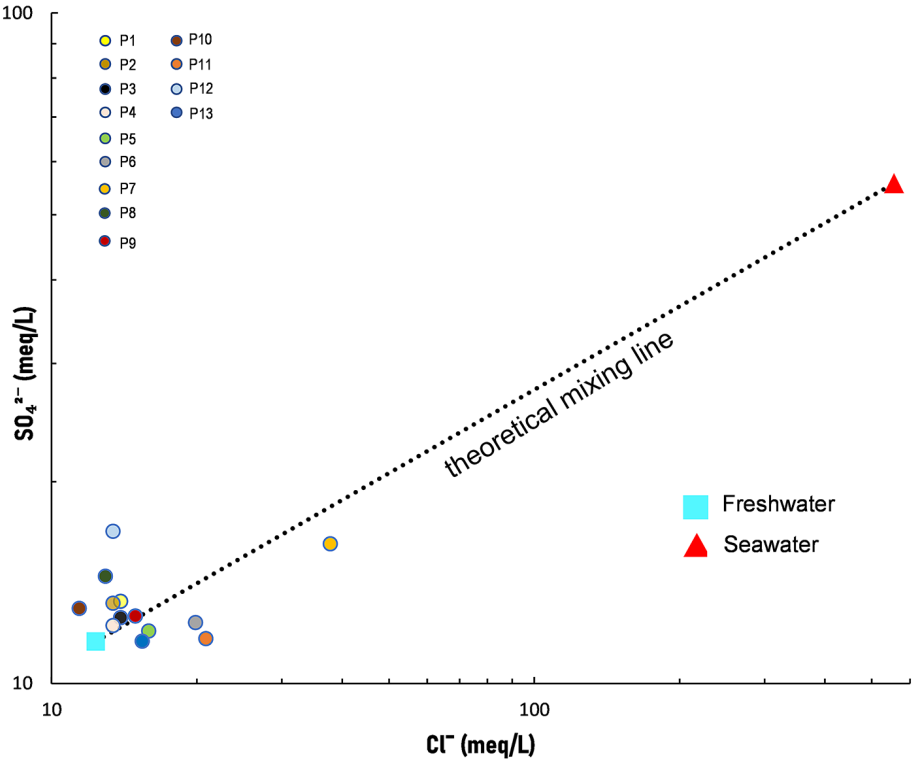

Fig. 12. Sulfate versus Chloride cross-plots of the Limnos volcan Ghiss-Nekor aquifer

Table 7. Hydrochemical facies of ONEP groundwater samples identified based on HFE plot

Hydrochemical facies	No. of samples	% samples	Sample location
MixNa-MixCl	5	38.46%	P1, P2, P5, P9, P13
MixCa-MixCl	2	15.38%	P3, P4
MixNa-Cl	2	15.38%	P11, P6
Na-Cl	1	7.69%	P7
MixNa-MixSO4	3	23.08%	P8, P10, P12

chemical behavior of chloride, the molar ratios of NO_3/Cl have often served to highlight and distinguish the various sources of nitrate in groundwater. In this study, the NO_3/Cl ratios ranged between 0.00275 and 0.037 with an average of 0.017. The plot of NO_3^-/Cl^- ratios versus Cl^- content (Fig. 13a) shows that the distribution of nitrate in the study area is significantly affected by various land uses or anthropogenic activities. Most of the investigated groundwater samples exhibited high Cl concentrations along with lower NO_3/Cl ratios; which reflects the involvement of septic effluents or organic matter such as manure in the release of both chloride and nitrate. The NO_3/Cl ratios rapidly increased to reach the maximum value in the vicinity of the uncontrolled landfill site where groundwater is characterized by elevated concentrations of nitrate (>50 mg/L) and chloride (>1000 mg/L); this is likely due to the impact of leachate infiltration. On the other hand, the low NO_3/Cl ratios, low K^+ values and the weak correlation between NO_3^- and K^+ -Table 8- indicate the minor influence of agricultural sources. A localized increase in boron contents occurred in the groundwater sampled near the landfill site, which likely reflects the influence of leachate seepage (Fig. 13b). The amounts of boron decrease with increasing distance from the landfill site; however, boron concentration tended to increase slightly in the wellfield located along the Ghiss River bank characterized by local agricultural practices and the proximity of effluents from residential septic tanks. The linearity and positive correlation between boron and nitrate (0.82), as well as chloride and boron (0.79) also emphasize the influence of anthropogenic inputs (Table 8) (Qin, 2019).

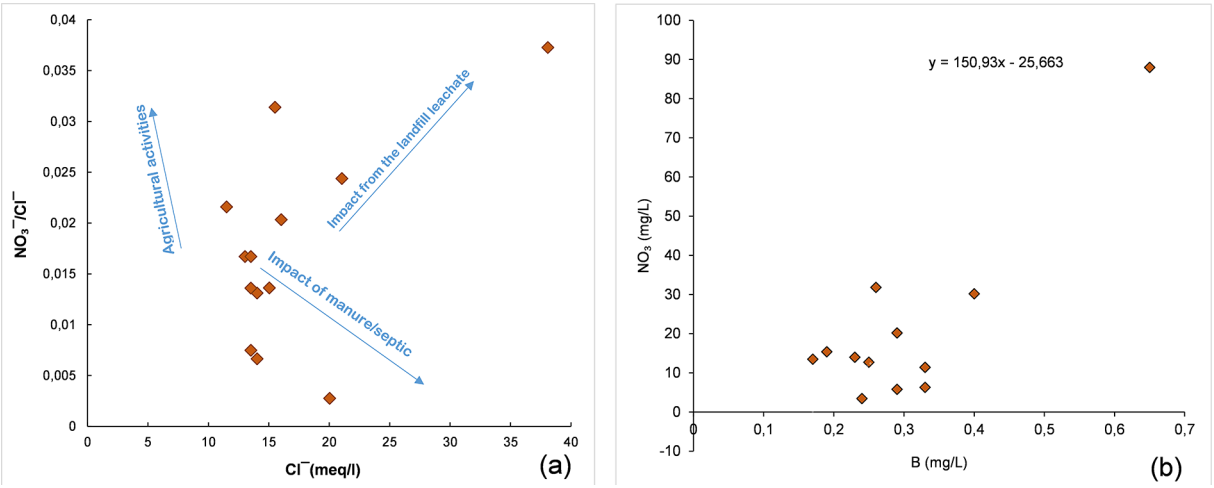

Fig. 13. Plots of (a) Cl versus NO_3/Cl molar ratio (b) variations of NO_3− with Boron contents

Table 8. Correlation coefficients between WQI and water-quality parameters

	DO	Turbidity	EC	TDS	Cl^-	HCO_3^-	SO_4^{2-}	NO_3^-	F^-	Ca^{2+}	Mg^{2+}	B^{3+}	Na^+	K^+	pH	WQI	SPI
DO	1																
Turbidity	0.061	1															
EC	-0.069	0.786	1														
TDS	-0.069	0.786	1	1													
Cl^-	-0.003	0.881	0.922	0.922	1												
HCO_3^-	-0.415	0.699	0.551	0.551	0.637	1											
SO_4^{2-}	-0.382	0.282	0.559	0.559	0.366	0.169	1										
NO_3^-	0.091	0.930	0.861	0.861	0.901	0.683	0.435	1									
F^-	-0.065	0.118	0.096	0.096	0.165	0.237	-0.075	0.143	1								
Ca^{2+}	0.113	0.670	0.736	0.736	0.695	0.309	0.570	0.772	-0.263	1							
Mg^{2+}	-0.193	0.225	0.166	0.166	0.333	0.467	0.012	0.308	0.109	0.398	1						
B^{3+}	-0.279	0.837	0.664	0.664	0.798	0.935	0.254	0.827	0.186	0.501	0.459	1					
Na^+	0.121	0.655	0.783	0.783	0.822	0.440	0.473	0.803	0.023	0.647	0.355	0.573	1				
K^+	-0.030	0.133	-0.123	-0.123	0.132	0.476	-0.495	0.124	0.084	-0.020	0.691	0.436	0.106	1			
pH	0.144	0.002	0.216	0.216	-0.015	-0.049	0.262	0.209	-0.340	0.474	0.013	-0.017	0.074	-0.061	1		
WQI	-0.105	0.862	0.947	0.947	0.963	0.690	0.531	0.939	0.117	0.783	0.398	0.818	0.853	0.108	0.148	1	
SPI	-0.143	0.876	0.689	0.689	0.835	0.903	0.217	0.876	0.212	0.545	0.465	0.989	0.623	0.444	0.003	0.843	1

Note: *correlation is significant at the 0.05 level, **correlation is significant at the 0.01 level.

Enrichment or depletion patterns of SO_4^{2-} and NO_3^-

The average values corresponding to ΔSO_4^{2-} and ΔNO_3^- were, respectively, 1.71 and 0.26. As Fig .14 illustrates, the values of ΔSO_4^{2-} were generally positive; SO_4 enrichment prevails in 92% of groundwater samples. On the other hand, the nitrate ionic deltas were close to zero in most groundwater samples which demonstrates that NO_3^- ion approaches conservative behavior, except for three samples (locations P7, P11, P13) exhibiting a pronounced NO_3^- enrichment given the impact of anthropogenic pollution. The positive trend of ΔSO_4 in the northwestern wellfield and some inland water samples is likely due to the release of evaporates disseminated through the Nekor basin in addition to sewage input and contaminant loadings provided by anthropogenic activities. The latter case is explained by the fact that the sulfate input increased sharply towards septic tank systems, residential areas and near the landfill site where Cl^- and NO_3 enrichment were also observed.

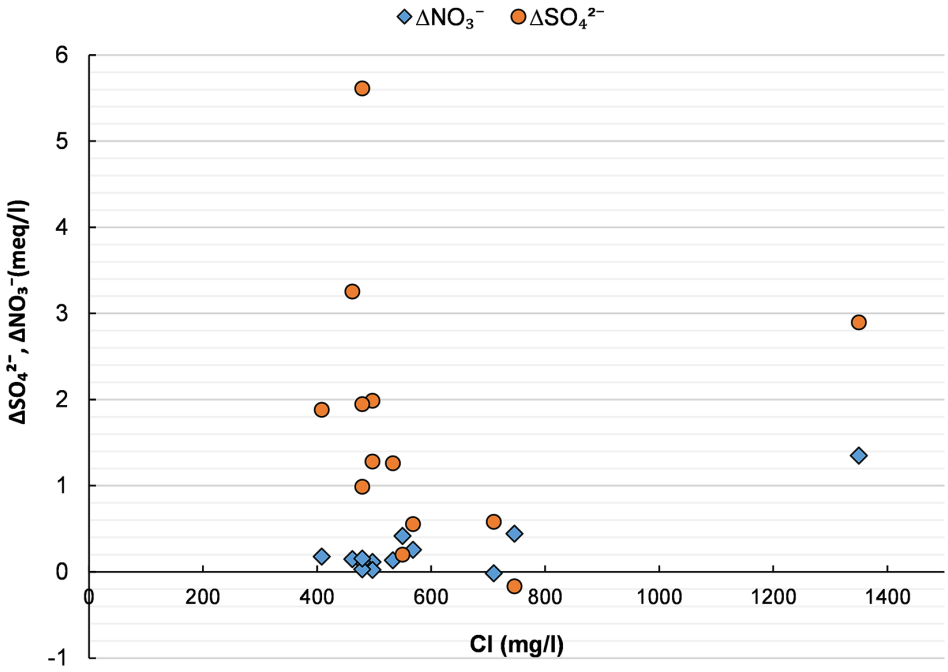

Fig. 14. Relationship between the amount of excess/depletion of NO_3 and SO_4

CONCLUSIONS

Groundwater quality in the Ghiss-Nekor coastal plain seems to reveal the combined influence exerted by the lithological nature of the aquifer, human activities and land use practices. This work enabled drawing the following conclusions: (1) all of the wells investigated in this study contained brackish groundwater (TDS>1000 mg/l); accordingly, it is only suitable for irrigation, (2) the HFE-D plot and the chloro-alkaline indices indicated the prevalence of the salinization geochemical trend and the dominance of reverse ion exchange process in the study area, respectively, (3) high levels of various dissolved constituents (notably Cl^-, TDS, and NO_3^-) generated high scores of WQI, reflecting the absence of potable water, (4) the majority of the water samples are either slightly or moderately polluted, as assessed by the synthetic pollution index, (5) although the excessive groundwater extraction and coarse deposits favored the occurrence of saltwater intrusion, the latter phenomenon could not be enhanced in the northwestern edge given the presence of thin bands of silt or clay creating a natural barrier that prevents the upward movement of seawater, (6) besides the impact of natural weathering processes on groundwater quality (marked by the enrichment of sulfate), anthropogenic origin was also demonstrated by the significant correlation between the high NO_3^- and Cl^- concentrations emanating from septic tank and landfill leachates or agricultural practices for higher NO_3/Cl ratios. Therefore, the groundwater within the Ghiss-Nekor aquifer was found to be unreliable for direct consumption without a proper prior treatment. Groundwater is unsafe for drinking, notably around Beni Bouayach uncontrolled landfill given the absence of impermeable clayey protective unit; hence, priority should be given to protecting this vulnerable site against further deterioration of groundwater quality by investigating a new controlled landfill in the least vulnerable areas where the aquifer is protected by relatively impermeable layers. The present study provided useful findings that may serve as a baseline for future research and to improve decision making. However, the conducted study is subject to certain limitations such as not incorporating an evaluation of temporal patterns variation of groundwater quality. In addition, the selected data are sparsely distributed, which made it difficult to carry out a robust spatial interpolation.

Acknowledgements

Hereby, the authors thank and acknowledge the national governmental organizations namely: Water Quality Service of the Morocco's National Office of Potable Water (ONEP) and the Loukkos

Hydraulic Basin Agency (ABHL) for providing the necessary data (water-quality and quantity monitoring data) for this research, for helping with the data preprocessing and for sharing a number of relevant references, as well as the Centre of Scientific and Technical Research in Morocco (CNRST) for funding this research. This research was supported with funds from the Centre of Scientific and Technical Research in Morocco (CNRST) under research phD grant No. 5UIT2018.

REFERENCES

1. Abdouni A.E., Bouhout S., Merimi I., Hammouti B. and Haboubi K. 2021. Physicochemical characterization of wastewater from the Al-Hoceima slaughterhouse in Morocco. Caspian Journal of Environmental Sciences, 3(19), 423-429.
2. Abu-Alnaeem M.F., Yusoff I., Ng T.F., Alias Y. and Raksmey M. 2018. Assessment of groundwater salinity and quality in Gaza coastal aquifer, Gaza Strip, Palestine: An integrated statistical, geostatistical and hydrogeochemical approaches study. Science of the Total Environment, 615, 972-989.
3. Adimalla N., Dhakate R., Kasarla A. and Taloor A.K. 2020. Appraisal of groundwater quality for drinking and irrigation purposes in Central Telangana, India. Groundwater for Sustainable Development, 10, 100334.
4. Aghazadeh N. and Mogaddam A.A. 2010. Assessment of groundwater quality and its suitability for drinking and agricultural uses in the Oshnavieh Area, Northwest of Iran. J. Environ. Prot., 01(1), 30.
5. Akoteyon I.S., Balogun I.I. and Soneye A.S.O. 2018. Integrated approaches to groundwater quality assessment and hydrochemical processes in Lagos, Nigeria. Applied Water Science, 8, 1-19.
6. Al Naeem M.F.A., Yusoff I., Ng T.F., Maity J.P., Alias Y., May R. and Alborsh H. 2019. A study on the impact of anthropogenic and geogenic factors on groundwater salinization and seawater intrusion in Gaza coastal aquifer, Palestine: An integrated multi-techniques approach. Journal of African Earth Sciences, 156, 75-93.
7. Andaloussi K., Achtak H., Nakhcha C., Haboubi K. and Stitou M. 2021. Assessment of soil trace metal contamination of an uncontrolled landfill and its vicinity: the case of the city of 'Targuist'(Northern Morocco). Moroccan Journal of Chemistry, 3(9), 9-3, 2513-2529.
8. Armugha Khan, Himanshu Govil, Ajay Kumar Taloor and Gaurav Kumar. 2020. Identification of artificial groundwater recharge sites in parts of Yamuna River basin India based on Remote Sensing and Geographical Information System. Groundw. Sustain. Dev., 11, 100415.
9. Ayyandurai R., Venkateswaran S. and Karunanidhi D. 2022. Hydrogeochemical assessment of groundwater quality and suitability for irrigation in the coastal part of Cuddalore district, Tamil Nadu, India. Marine Pollution Bulletin, 174, 113258.
10. Belghiti M., Chahlaoui A., Bengoumi D. and El Moustaine R. 2013. Study of the physico- chemical and bacteriological quality of the groundwater of the plio-quaternary aquifer in the Meknes region (Morocco). Larhyss Journal, 14.
11. Benabdelouahab S., Salhi A., Himi M., Stitou El Messari J.E. and Casas Ponsati A. 2019. Geoelectrical investigations for aquifer characterization and geoenvironmental assessment in northern Morocco. Environmental earth sciences, 78, 1-16.
12. Benaissa C., Bouhmadi B., Rossi A. and El Hammoudani Y. 2020. Hydro-chemical and bacteriological Study of Some Sources of Groundwater in the GHIS-NEKOR and the BOKOYA Aquifers (AL HOCEIMA, MOROCCO). Proc of The 4th Edition of International Conference on Geo-IT and Water Resources, 1-5.
13. Benaissa C., Bouhmadi B., Rossi A., El Hammoudani Y. and Dimane F. 2022. Assessment of Water Quality Using Water Quality Index – Case Study of Bakoya Aquifer, Al Hoceima, Northern Morocco. Ecological Engineering & Environmental Technology, 4(23), 31-44.
14. Bodrud-Doza M., Bhuiyan M.A H., Islam S.D.-U., Rahman M.S., Haque M.M., Fatema K.J., Ahmed N., Rakib M. and Rahman M.A. 2019. Hydrogeochemical investigation of groundwater in Dhaka City of Bangladesh using GIS and multivariate statistical techniques. Groundw. Sustain. Dev., 8, 226-244.
15. Bouhout S., Haboubi K., El Abdouni A., El Hammoudani Y., Haboubi C., Dimane F., Hanafi I. and Elyoubi M.S. 2023. Appraisal of Groundwater Quality Status in the Ghiss-Nekor Coastal Plain. Journal of Ecological Engineering, 10(24).
16. Bouhout S., Haboubi K., Zian A., Elyoubi M.S. and Elabdouni A. 2022. Evaluation of two linear kriging methods for piezometric levels interpolation and a framework for upgrading groundwater level monitoring network in Ghiss-Nekor plain, north-eastern Morocco. Arabian Journal Geosciences, 10(15), 1-17.
17. Bourjila A., Dimane F., Ghalit M., Taher M., Kamari S., El Hammoudani Y., Achoukhi I. and Haboubi K. 2023. Mapping the spatiotemporal evolution of seawater intrusion in the Moroccan coastal aquifer of Ghiss-Nekor using GIS-based modeling. Water Cycle, 4, 104-119.
18. Bourjila A., Dimane F., Ouarghi H.E., Nouayti N., Taher M., Hammoudani Y.E., Saadi O. and Bensiali A. 2021. Groundwater potential zones mapping by applying GIS, remote sensing and multi-criteria

decision analysis in the Ghiss basin, northern Morocco. Groundw. Sustain. Dev., 15, 100693.

19. Chukwu A.C., Chibuike A., Njoku O.P. and Anthony C. 2023. Integrated electrical resistivity methods for evaluation of fracture terrain groundwater potentials, case study of indurated shale of Lower Benue trough, Southeastern Nigeria. Groundwater for Sustainable Development, 101014.
20. Das C.R., Das S. and Panda S. 2023. MLR index–based principal component analysis to investigate and monitor probable sources of groundwater pollution and quality in coastal areas: a case study in East India. Environmental Monitoring and Assessment, 10(195), 1158.
21. Dimane F. and El Hammoudani Y. 2021. Assessment of quality and potential reuse of wastewater treated with conventional activated sludge. Materials Today: Proceedings, 45, 7742-7746.
22. Dimane F., Haboubi K., Hanafi I., El Himri A. and Aridaloussi K. 2017. Impact des facteurs de pollution sur la qualité des eaux de la zone aval de la vallée de l'oued Nekor (Al-Hoceima, Maroc). European Scientific Journal, 3(13), 44-60.
23. El Abdouni A., Bouhout S., Merimi I., Hammouti B. and Haboubi K. 2021. Physicochemical characterization of wastewater from the Al-Hoceima slaughterhouse in Morocco. Caspian Journal of Environmental Sciences, 3(19), 423-429.
24. El Hammoudani Y. and Dimane F. 2020. Assessing behavior and fate of micropollutants during wastewater treatment: Statistical analysis. Environmental Engineering Research, 5(26).
25. El Hammoudani Y. and Dimane F. 2021. Occurrence and fate of micropollutants during sludge treatment: Case of Al-Hoceima WWTP, Morocco. Environmental Challenges, 1(5), 1-8.
26. El Hammoudani Y., Dimane F. and El Ouarghi H. 2019. Fate of Selected Heavy Metals in a Biological Wastewater Treatment System. Euro-Mediterranean Conference for Environmental Integration, 157-163.
27. El Hammoudani Y., Dimane F., Haboubi K., Bourjila A., Benaissa C., Achoukhi I. and Haboubi C. 2023. Assessment of Groundwater Quality in the Lower Wadi of The Nekor Valley, Al-Hoceima-Morocco. Environmental Engineering & Management Journal (EEMJ), 3(22).
28. Elabdouni A., Haboubi K., Bensitel N., Bouhout S., Aberkani K. and El Youbi M.S. 2022. Removal of organic matter and polyphenols in the olive oil mill wastewater by coagulation-flocculation using aluminum sulfate and lime. Moroccan Journal of Chemistry, 1(10), 191-202.
29. Elabdouni A., Haboubi K., Merimi I. and El Youbi M. 2020. Olive mill wastewater (OMW) production in the province of Al-Hoceima (Morocco) and their physico-chemical characterization by mill types. Materials Today: Proceedings, 27, 3145-3150.
30. Errahmouni A., El Messari J.E.S. and Taher M. 2022. Estimation of groundwater recharge using APLIS method–case study of Bokoya Massif (Central Rif, Morocco). Ecological Engineering & Environmental Technology, 23.
31. Errahmouni A., Gharibi E., Ghalit M. and Taupin J. 2017. Caractérisation hydrochimique des eaux souterraines situées dans le massif de Bokoya (Rif central, Maroc). ColloqueInternationalEau–Société-Climat'2017 (ESC-2017).
32. Ferchichi H., Ben Hamouda M., Farhat B. and Ben Mammou A. 2018. Assessment of groundwater salinity using GIS and multivariate statistics in a coastal Mediterranean aquifer. Int J Environ Sci Technol, 15, 2473-2492.
33. Fernine Y., Arrousse N., Haldhar R., Raorane C.J., Kim S.-C., El Hajjaji F., Touhami M.E., Beniken M., Haboubi K. and Taleb M. 2022. Synthesis and characterization of phenolphthalein derivatives, detailed theoretical DFT computation/molecular simulation, and prevention of AA2024-T3 corrosion in medium 3.5% NaCl. Journal of the Taiwan Institute of Chemical Engineers, 140, 104556.
34. Gad M., Saleh A. H., Hussein H., Farouk M. and Elsayed S. 2022. Appraisal of surface water quality of nile river using water quality indices, spectral signature and multivariate modeling. Water, 7(14), 1131.
35. Gao Y., Qian H., Ren W., Wang H., Liu F. and Yang F. 2020. Hydrogeochemical characterization and quality assessment of groundwater based on integrated-weight water quality index in a concentrated urban area. Journal of cleaner production, 260, 121006.
36. Ghalit M., Yousfi E., Zouhairi M., Gharibi E. and Taupin J. 2017. Hydrochemical characterization of groundwater in the Nekor basin located in the North-East of the Rif of Morocco. Moroccan Journal of Chemistry, 2(5), 5-2 (2017) 2272-2284.
37. Hajji S., Allouche N., Bouri S., Aljuaid A.M. and Hachicha W. 2022. Assessment of seawater intrusion in coastal aquifers using multivariate statistical analyses and hydrochemical facies evolution-based model. Int. J. Environ. Res. Public Health., 1(19), 155.
38. Jha M.K., Shekhar A. and Jenifer M.A. 2020. Assessing groundwater quality for drinking water supply using hybrid fuzzy-GIS-based water quality index. Water Research, 179, 115867.
39. Kadam A., Wagh V., Jacobs J., Patil S., Pawar N., Umrikar B., Sankhua R. and Kumar S. 2022. Integrated approach for the evaluation of groundwater quality through hydro geochemistry and human health risk from Shivganga river basin, Pune, Maharashtra, India. Environmental Science and Pollution Research, 3(29), 4311-4333.
40. Kanga I., Naimi M. and Chikhaoui M. 2020. Groundwater quality assessment using water quality

index and geographic information system based in Sebou River Basin in the North-West region of Morocco. International Journal of Energy and Water Resources, 4(4), 347-355.

41. Krivoruchko K. (2011). Spatial statistical data analysis for GIS users, Esri Press Redlands.
42. Laonamsai J., Pawana V., Chipthamlong P., Chomcheawchan P., Kamdee K., Kimmany B. and Julphunthong P. 2023. Groundwater Quality Variations in Multiple Aquifers: A Comprehensive Evaluation for Public Health and Agricultural Use. Geosciences, 7(13), 195.
43. Neverre N., Surdyk N., Hérivaux C. and Baran N. 2022. Restoring groundwater quality at the drinking water catchment scale: A multidisciplinary and participatory approach. Journal of Environmental Management, 314.
44. Ngouala M., Mbilou U., Tchoumou M. and Samba-Kimbata M. 2016. Characterization Surface Water-Groundwater Aquifer in Coastal Watershed of the Republic of Congo Loémé. Larhyss Journal, 28, 237-256.
45. Ouhamdouch S., Bahir M. and Ouazar D. 2021. Seawater intrusion into coastal aquifers from semi-arid environments, Case of the alluvial aquifer of Essaouira basin (Morocco). Carbonates and Evaporites, 36, 1-12.
46. Purwoarminta A., Moosdorf N. and Delinom R.M. 2018. Investigation of groundwater-seawater interactions: a review. IOP Conference Series: Earth and Environmental Science, 012017.
47. Radouane E.M., Chahlaoui A., Maliki A. and Boudellah A. 2023. Assessment and modeling of groundwater quality by using water quality index (WQI) and GIS technique in meknes aquifer (Morocco). Geology, Ecology, and Landscapes, 2(7), 126-138.
48. Rodier J., Bernard L. and Nicole M. (2009). Water analysis, natural water, wastewater, seawater, 9th edn (Dunod, Paris, 2009), ISBN 987-2-10-054179-9.
49. Rupias O.J.B., Pereira S.Y. and de Abreu A.E.S. 2021. Hydrogeochemistry and groundwater quality assessment using the water quality index and heavy-metal pollution index in the alluvial plain of Atibaia river-Campinas/SP, Brazil. Groundwater for Sustainable Development, 15, 100661.
50. Saleh A., Gad A., Ahmed A., Arman H. and Farhat H.I. 2023. Groundwater Hydrochemical Characteristics and Water Quality in Egypt's Central Eastern Desert. Water, 5(15), 971.
51. Salhi A. 2008. Geophysics, Hydrogeology And Mapping. PhD. Thesis, Ecole Normale Supérieure.
52. Shukla A.K., Ojha C. and Garg R. (2017). Application of overall index of pollution (OIP) for the assessment of the surface water quality in the upper Ganga river basin, India. Development of Water Resources in India, Springer**:** 135-149.
53. Solangi Y.A., Tan Q., Mirjat N.H. and Ali S. 2019. Evaluating the strategies for sustainable energy planning in Pakistan: An integrated SWOT-AHP and Fuzzy-TOPSIS approach. Journal of Cleaner Production, 236, 117655.
54. Yifru B.A., Mitiku D.B., Tolera M.B., Chang S.W. and Chung I.-M. 2020. Groundwater potential mapping using SWAT and GIS-based multi-criteria decision analysis. KSCE Journal of Civil Engineering, 8(24), 2546-2559.
55. Zghibi A., Merzougui A., Chenini I., Ergaieg K., Zouhri L. and Tarhouni J. 2016. Groundwater vulnerability analysis of Tunisian coastal aquifer: an application of DRASTIC index method in GIS environment. Groundw. Sustain. Dev., 2, 169-181.